Coherent isotropic averaging in zero-field nuclear magnetic resonance. I. General theory and icosahedral sequences

A. Llor,[a] Z. Olejniczak,[b] and A. Pines
Materials Sciences Division, Lawrence Berkeley Laboratory, and Department of Chemistry, University of California, Berkeley, California 94720

(Received 23 January 1995; accepted 25 May 1995)

We present a general theory of coherent isotropic averaging in nuclear magnetic resonance (NMR). In a zero external field, magnetic-field pulses can selectively average the internal spin Hamiltonians, while preserving the intrinsic invariance of the spectrum with respect to the sample orientation. The theory predicts the limits of the scaling factors for tensor interactions of different ranks. Time reversal is found to be possible for first- and second-rank tensors with scaling factors of $-1/3$ and $-1/4$, respectively. Explicit sequences, based on icosahedral symmetry, are given for a number of optimal scaling factors. To illustrate the theory, an experiment is also presented in the special case of rank-selective decoupling. As in high-field NMR, applications can be expected from the introduction of coherent averaging schemes for zero-field techniques: for example, decouplings (by rank or nuclear species), time reversal, and multipolar experiments (zero-field analog of multiple-quantum NMR). © *1995 American Institute of Physics.*

I. INTRODUCTION

The importance of NMR as an analytical tool derives from its ability to provide atomic and molecular information about a sample through the measurement of intrinsic nuclear spin couplings. However, these are not observed alone but in conjunction with the Zeeman interaction, which truncates them in an anisotropic way.[1,2] The truncated local couplings depend upon the orientation of the privileged local directions (for instance, crystalline axes) with respect to the magnetic field. Since many available solid-state samples are polycrystalline or amorphous, they yield powder spectra in which the anisotropy broadening often obscures any potentially resolvable features.

To overcome this difficulty, various techniques of solid state NMR have been developed over the last three decades, including ''magic-angle'' spinning (MAS),[3] multiple-pulse irradiation sequences (for example, WHH),[4] and more recently, dynamic-angle spinning (DAS),[5] and double rotation (DOR).[6] By using such techniques, the anisotropic parts of the interactions are averaged out and the resolution of the spectra can become similar to that obtained from liquid samples.[2–7] These methods involve sample reorientations and coherent radiofrequency irradiations whose effects can be described in terms of coherent-averaging theory.[7] Coherent averaging allows for a wide range of Hamiltonian manipulations, where different terms can be modified according to magnetogyric ratio (as in heteronuclear decoupling) or tensor rank (as in WHH). Sign changes, known as time reversals, have also been performed (as in Hahn echo[8] and magic echo experiments[9]) and they are essential for phase coherence in multiple-quantum NMR and other forms of two-dimensional conjugate detection.[10]

Although the use of high-resolution tools of solid-state NMR enhances the information content of the spectra, it leads to some loss of information as well. The anisotropic parts of the broadening are due to contributions from the local couplings whose observation can be as valuable. An alternative approach, zero-field NMR (ZF-NMR), was introduced a few years ago to address this problem.[11] In contrast with many spectroscopies, ZF-NMR has no privileged direction in the laboratory frame since the magnetic field is removed, and thus all the crystallites of the sample are equivalent. For powder samples, the resolution of observed spectra is similar to what would be obtained from standard high-field NMR on the corresponding single crystals. ZF-NMR is closely related to nuclear quadrupolar resonance (NQR),[12] but it is a coherent technique where the signal is recorded in the time domain, yielding the spectrum after Fourier transformation. As shown in Fig. 1, the evolution in a zero field is initiated and stopped by sudden transitions of the magnetic field, whereas to monitor the signal, nuclear polarization is created and observed in a high field. Through field cycling, this exploits the isotropic behavior in a zero field, while preserving the sensitivity of standard NMR. We shall use the term ''high-field NMR,'' or HF-NMR, for the usual NMR spectroscopy where the Zeeman interaction is much stronger than the local interactions.

An intermediate solution has been developed recently, the ''zero field in high field'' NMR, or ZFHF.[13,14] This coherent averaging method combines sample rotation and radiofrequency irradiation *performed completely in a high field* and makes the system evolve *as if it were in a zero field*. This ''untruncation'' technique has many advantages over the pure ZF-NMR, since no field cycling is necessary and heteronuclear species can be easily decoupled, but it is limited by the maximum achievable spinning rate of the sample (currently up to 30 kHz in the state-of-the-art turbines).

Although coherent averaging methods are now well known and understood in HF-NMR (for decoupling, time reversal, etc.), there is an almost complete lack, so far, of similar techniques in zero-field spectroscopy. Indeed, aside

[a]Present address: 5, rue Saint Denis, 92100 Boulogne, France.
[b]Present address: Radiospectroscopy Division, Institute of Nuclear Physics, Radzikowskiego 152, 31-342 Kraków, Poland.

 0021-9606/95/103(10)/3966/16/$6.00

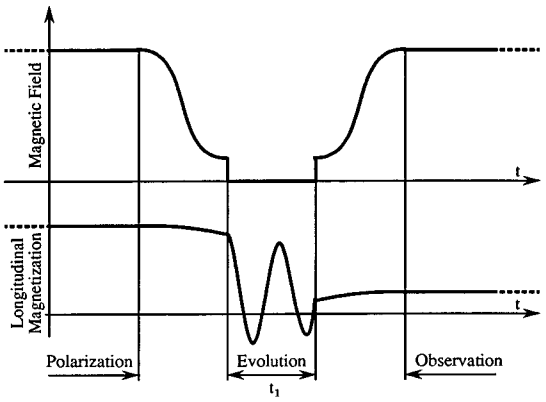

FIG. 1. Schematic description of the zero-field NMR (ZF-NMR) experiment (Ref. 11). Through magnetic-field cycling, the evolution of the nuclei under the influence of the untruncated local interactions in the zero field is recorded in the high field, with the corresponding sensitivity enhancement. The evolution is initiated and terminated by suddenly switching the magnetic field. This is a coherent transient experiment, where the zero-field evolution is recorded point by point and the spectrum is obtained after the Fourier transformation with respect to time t. Since strong magnets cannot be switched rapidly enough, a two-step cycling of the field is performed: first, in about 200 ms, to an intermediate value ($\approx$10 mT) generated by an auxiliary coil, which, in turn, can be switched in less than 1 μs.

from single crystal cases, coherent irradiation schemes have been limited to excitation and echo techniques,[12,15–17] and to a theoretical exploration of some specific homonuclear decoupling sequences.[18,19] NQR echoes, which were introduced shortly after the HF-NMR Hahn echo,[15] are not evolved under a well defined truncation axis in the laboratory frame. In a polycrystalline sample, the orientations of the local quadrupolar interactions are randomly distributed, inducing correspondingly different matrix elements of the irradiation field.[12] The evolution in a powder sample during a NQR echo is only approximately refocused and, in contrast to the HF-NMR Hahn and magic echoes, it cannot be used as a building block to generate coherent irradiation sequences. Compensation schemes for these imperfections have not been implemented to manipulate spin interactions in a zero field, but some echo-train techniques have been used to improve the signal detection or perform two-dimensional experiments.[16,17]

Coherent manipulations of the local interactions in ZF-NMR can be performed using magnetic field pulses, traditionally called ''dc pulses.''[18] Unlike an rf pulse in NQR, a dc pulse in ZF-NMR can excite the whole spectrum, just as the initial magnetic field transient does (Fig. 1). Furthermore, since the field during the pulse is stronger than the local interactions, its effect can be conveniently described as a spin rotation. By analogy with pulse schemes in HF-NMR,[4,7] zero-field homonuclear decoupling sequences have been developed using $\pi/2$ rotations along the three reference axes.[18,19] These averaging processes, which we shall call ''cubic,'' were designed for the full zero-field Hamiltonians, regardless of the crystallite orientations. In their δ-pulse versions, the cubic sequences involved 4 or 12 $\pi/2$ pulses for interactions transforming under spin rotations as first- or second-rank tensors, respectively.

By analogy with the HF-NMR case, the development of general coherent methods in ZF-NMR can be seen as a useful step in expanding the possible applications of NMR in solids. The present article is thus devoted to an important class of coherent processes in ZF-NMR that we term *coherent isotropic averaging*. Some preliminary examples were introduced in a recent letter,[20] with applications to time-reversal experiments. Here, we shall extensively discuss the concept of isotropic averaging, providing the group theoretical foundations of the theory. Symmetry considerations make it possible to solve the theoretical problem in the general case, and provide ''canonical'' sequences based on icosahedral distributions. The special case of decoupling sequences will then be examined, together with the general high-field isotropic sequences. In conclusion, possible applications of isotropic scaling in ZF-NMR and NQR will be briefly discussed (decoupling, multipolar analysis, imaging,...), and we shall make some general comments on time-reversal scalings. An experiment based on an icosahedral sequence will also be reported in this paper, but the practically useful cubic sequences are relegated to a subsequent article, together with experimental considerations concerning finite pulse compensations.

II. GENERAL CONCEPT OF ISOTROPIC TRAJECTORY

The starting point is the general problem of *isotropic scaling*: How can we perform a scaling of the complete zero-field Hamiltonian while preserving the isotropic behavior of ZF-NMR. This may not seem very useful in general, except in the ZFHF sequence, which performs an isotropic scaling (starting with a truncated anisotropic interaction) in the experiment carried out completely in a high field.[13,14] As we shall see, however, different parts of the Hamiltonian, distinguished by rank of interactions or nuclear species, can be scaled by different factors. Then, WHH-like schemes (to decouple second-rank interactions while retaining first-rank interactions, or vice versa), time reversal, or heteronuclear decoupling become special cases of scaling-factor combinations, and they can be more clearly visualized and understood from the broader framework of isotropic scaling. We shall devote most of the present article to the homonuclear case (like spins).

In a high-field NMR, coherent manipulations of the Hamiltonian are achieved by applying radio-frequency pulses (modulated in phase, frequency or amplitude) and sample reorientations (using a turbine, for example).[2,7] In a zero field, however, there is no Zeeman interaction and accordingly the spins have to be excited with dc pulses of the magnetic field, in such a way that all the transitions of the system are effectively covered up to the cutoff frequency corresponding to the pulse duration.[18] Since there is no rotating frame, there is no equivalent to the phase modulations of HF-NMR, and pulses along different axes must be generated by physically applying dc pulses along these orientations. Thus zero-field coherent processes require a set of at least two, and more conveniently three, crossed coils to generate any type of pulse. On the other hand, it can be shown[18] (see Sec. VI) that sample reorientation is not necessary in a zero field. It can always be imitated by applying dc pulses,

which are significantly more efficient than reorientation. We shall thus describe all the zero-field coherent processes in terms of magnetic-field pulses only.

As a brief reminder of the main ingredients of coherent averaging theory,[7] consider the case of a δ-pulse sequence, under which the system evolves due to the zero-field Hamiltonian $H_0(\Omega)$ (where Ω represents the orientation of the local interaction axes in the laboratory frame) during $n+1$ time intervals t_i $(0 \leqslant i \leqslant n)$, separated by n pulses whose effects are given by rotation operators P_i in the spin space. The evolution of the system over one sequence cycle, in the first order,[21] is determined by the average Hamiltonian

$$\overline{H^{(1)}}(\Omega) = \sum_{0 \leqslant i \leqslant n} (R_i \cdot H_0(\Omega) \cdot R_i^{\dagger}) t_i / t_c$$

$$= \sum_{0 \leqslant i \leqslant n} H_i(\Omega) t_i / t_c = \langle H_i(\Omega) \rangle, \tag{1}$$

where the bracket notation in the last expression stands for the average over i. The rotations applied to the Hamiltonian, R_i, are related to the pulses according to

$$R_i = (P_i \cdot P_{i-1} \cdot \cdots \cdot P_2 \cdot P_1)^{\dagger} \quad \text{or} \quad P_i = R_i^{\dagger} \cdot R_{i-1}, \tag{2}$$

with the supplementary condition of a cyclic sequence

$$R_n = (P_n \cdot P_{n-1} \cdot P_{n-2} \cdot \cdots \cdot P_3 \cdot P_2 \cdot P_1)^{\dagger} = I, \tag{3}$$

where I is the identity operator. According to the established terminology, we call the set of rotated Hamiltonians, $\{H_i(\Omega)\}$, the *trajectory in the operator space*. The $\{R_i\}$ will be called the *set of configurations or the configuration trajectory*, and it is the object that is the closest to $\{H_i(\Omega)\}$, which completely and uniquely defines the process. The rotation of operators defines a representation of the group of rotations, SO(3), on the space of operators, and thus $\{H_i(\Omega)\}$ is associated with $\{R_i\}$ through this group representation. For any $\{R_i\}$, the magnetic-field trajectory (i.e., the pulses $\{P_i\}$) will be given by Eq. (2). In the case of a practical sequence that does not consist of δ pulses (continuous, windowless or with pulses of finite width), the effect of the magnetic field can be accounted for by a continuous configuration trajectory $R(t)$, with the discrete sum in Eq. (1) replaced by an integral over $0 \leqslant t \leqslant t_c$. To visualize a trajectory, it is convenient to use the representation of the group of rotations, SO(3), as a sphere of radius π, where a rotation is represented by a vector pointing along the direction of the rotation axis and of a length equal to the magnitude of the total rotation angle.[22] Thus an ideal δ-pulse sequence, a windowless sequence, and a continuous trajectory are described, respectively, by a set of discrete points, a continuous line, and a continuous line without kinks (differentiable path) inside the SO(3) sphere as shown in Fig. 2.

The trajectory is called *isotropic* if it generates a zero-field-like average Hamiltonian, $\overline{H^{(1)}}(\Omega)$. This is the case, for instance, if the sequence performs the *scaling* of the local interaction $H_0(\Omega)$ by a factor k, independent of the orientation Ω

$$\overline{H^{(1)}}(\Omega) = \langle R_i \cdot H_0(\Omega) \cdot R_i^{\dagger} \rangle = k H_0(\Omega). \tag{4}$$

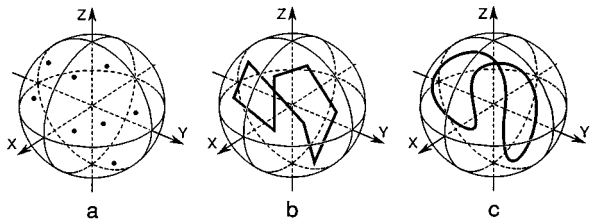

FIG. 2. Examples of trajectories in the configuration space SO(3) under various irradiation conditions: (a) for a δ-pulse sequence, (b) for a windowless pulse sequence, (c) for a sequence with a continuously modulated magnetic field. Each point in the sphere represents a rotation which acts on the Hamiltonian of the system.

Here, it must be emphasized that isotropic sequences are not necessarily scaling sequences. The important property in ZF-NMR is that the *eigenvalues* (but not the eigenstates) of the local Hamiltonian are independent of the crystallite orientation Ω. Thus we shall also call isotropic a sequence that at the same time scales and rotates the Hamiltonian.[13,14] Except in experiments where both the modified and free Hamiltonians are used successively, the effect of this rotation would be undetectable on a powder sample, and only transition intensities would be changed for a single crystal. This case of residual rotation is normally irrelevant since it can be compensated by two extra pulses. However, we do not rule out the possibility that some averaging schemes complying with the eigenvalue invariance may not be reduced to simple scalings by rotations. It can be shown that the applicability of such sequences would be restricted to some specific cases of interactions, generally involving limited numbers of levels. In the present work, we shall only analyze pure scaling sequences as defined by Eq. (4).

Before solving Eq. (4) explicitly, it is important to explore its symmetry properties. Starting from any given scaling sequence $\{R_i\}$, we can generate another trajectory using the transformation $\{U \cdot R_i \cdot V\}$, where U and V are fixed rotations. Defining $S = V^{\dagger}$ and $Q = U \cdot V$, we can rewrite the transformed configurations as $\{Q \cdot S \cdot R_i \cdot S^{\dagger}\}$, and according to the linearity of Eq. (4), the first order average Hamiltonian will become

$$\begin{aligned} H^{(1)}(\Omega) &= \langle (Q \cdot S \cdot R_i \cdot S^{\dagger}) \cdot H_0(\Omega) \cdot (Q \cdot S \cdot R_i \cdot S^{\dagger})^{\dagger} \rangle, \\ &= Q \cdot S \cdot \langle R_i \cdot H_0(S(\Omega)) \cdot R_i^{\dagger} \rangle \cdot S^{\dagger} \cdot Q^{\dagger}, \\ &= k Q \cdot S \cdot H_0(S(\Omega)) \cdot S^{\dagger} \cdot Q^{\dagger} = k H_0(Q^{-1}(\Omega)). \end{aligned} \tag{5}$$

When $Q = I$, the scaling behavior of a sequence is thus preserved under the transformation $\{S \cdot R_i \cdot S^{\dagger}\}$. The pulses are also rotated to $\{S \cdot P_i \cdot S^{\dagger}\}$ according to Eq. (2). This invariance can be intuitively understood by considering that the $\{R_i\}$ define some privileged directions in the laboratory frame, and that a scaling sequence must be independent of the initial choice of a reference frame. The other transformation, $\{Q \cdot R_i\}$, preserves the isotropic character of the couplings as well, but at the same time it does change the average Hamiltonian *unless the scaling factor is zero*. Thus in the configuration space, the invariance group for isotropic scal-

ing is SO(3), whereas for decoupling it is SO(3)×SO(3). As we shall see, these symmetry properties lead to different approaches to generating the corresponding scaling and decoupling sequences.

III. GENERAL SOLUTION TO THE ISOTROPIC-SCALING PROBLEM

As in HF-NMR,[7] the interactions are expanded into irreducible tensor representations,[22] since the effect of the pulses is described by rotations of the Hamiltonians. We shall consider only one such representation of order l, because in first order average Hamiltonian the contributions from different representations are just linearly superimposed. We thus write

$$H_0(\Omega)=\sum_m (-1)^m A_{l,-m}(\Omega)T_{lm}, \tag{6}$$

where the set of T_{lm} is a basis for the irreducible tensor operators, and $A_{lm}(\Omega)$ are the coefficients of the expansion which depend on the local axes orientation Ω (T_{lm} and $A_{lm}(\Omega)$ are also known as the spin and lattice parts, respectively). In the following, the rank l will be 1 (as for residual Zeeman couplings) or 2 (as for dipole–dipole and quadrupole couplings), though it might be higher in some special cases.[19] By introducing Wigner matrices[22] to describe the effect of the rotations $\{R_i\}$, we can rewrite Eq. (4) in the following way:

$$\sum_{mm'} \langle (-1)^m A_{l,-m}(\Omega)D^l_{m'm}(R_i)T_{lm'}\rangle$$

$$=k_l\sum_m (-1)^m A_{l,-m}(\Omega)T_{lm}, \tag{7}$$

where we show explicitly that the scaling factor may depend on the rank l. Since Eq. (7) must hold for any Hamiltonian of the given rank and for any orientation Ω, it must be valid whatever the coefficients $A_{l,-m}(\Omega)$. Thus

$$\langle D^l_{m'm}(R_i)\rangle = k_l\delta_{m'm}, \tag{8}$$

for any m and m' between $-l$ and l. The Ω dependence in Eq. (8) is now eliminated and the only remaining characteristic of the Hamiltonian is its rank l.

Now, the invariance properties of scaling sequences as given by Eq. (4) can be transferred to Eq. (8). The $\{R_i\}\rightarrow\{S\cdot R_i\cdot S^\dagger\}$ transformation translates into a linear transformation of the Wigner matrices $D^l_{mm'}(R_i)$

$$D^l_{m'm}(R_i)\rightarrow \mathbf{S}(D^l_{m'm}(R_i))$$

$$=\sum_{nn'} D^l_{m'n'}(S)D^l_{n'n}(R_i)D^l_{nm}(S^\dagger). \tag{9}$$

Actually, $\mathbf{S}$ can be applied to any $(2l+1)(2l+1)$ matrix M, according to

$$M_{m'm}\rightarrow \mathbf{S}(M_{m'm})=\sum_{nn'} D^l_{m'n'}(S)M_{n'n}D^l_{nm}(S^\dagger). \tag{10}$$

The relationship between S and $\mathbf{S}$ is thus a linear representation, known as the adjoint representation, of the group of rotations SO(3), in the space of linear transformations of the $(2l+1)$-dimensional vector space $\mathbf{L}(2l+1)$.[22,23] The representation formalism here is important, since the invariance property of Eq. (8) means precisely that the average $\langle D^l_{m'm}(R_i)\rangle$ belongs to the subspace of invariant irreducible representations in $\mathbf{L}(2l+1)$. We thus introduce $U_{\lambda\mu}$, the irreducible tensor basis for $(2l+1)(2l+1)$ matrices. $U_{\lambda\mu}$ can be chosen identical to the usual irreducible operator tensors of a spin l,[24] but we use a different notation, because the two tensors form the expansion bases of physically different objects that operate in different spaces: T_{lm} are used to expand Hamiltonians and operate over the spin space, whereas $U_{\lambda\mu}$ expand superoperators and act over the set of operators (which includes Hamiltonians and T_{lm}). The expansion of a Wigner matrix takes an especially simple form when the rotation is defined by its total rotation angle ω and its rotation axis $\mathbf{n}$[23,25]

$$D^l(R)=[4\pi/(2l+1)]^{1/2}\sum_{\lambda\mu} (-i)^\lambda \chi^l_\lambda(\omega)Y_{\lambda\mu}(\mathbf{n})U_{\lambda\mu}, \tag{11}$$

where $Y_{\lambda\mu}$ are the spherical harmonics, χ^l_λ are the generalized characters (χ^l_0 is the standard character χ^l), and the sum runs over $0\leqslant\lambda\leqslant 2l$ and $-\lambda\leqslant\mu\leqslant\lambda$. In Eq. (11) the $U_{\lambda\mu}$ tensors, whose matrix elements are proportional to the Clebsch–Gordan coefficients $C(\lambda\mu;lml'm')$,[25] are normalized by $\mathrm{Tr}(U^\dagger U)=1$.

Introducing expansion (11) for the $D^l_{m'm}(R_i)$ in Eq. (8), we obtain a set of relations

$$\langle \chi^l(\omega_i)\rangle = k_l(2l+1), \tag{12a}$$

$$\langle \chi^l_\lambda(\omega_i)Y_{\lambda\mu}(\mathbf{n}_i)\rangle = 0 \quad \text{for any } 1\leqslant\lambda\leqslant 2l \text{ and } -\lambda\leqslant\mu\leqslant\lambda. \tag{12b}$$

The first equation [which, incidentally, can be deduced directly by calculating the trace of Eq. (8)] gives a simple relationship between the scaling factor and the configuration trajectory: It is the *average of a function of the configuration rotation angle, regardless of the rotation axis*. By substituting the explicit expressions for the $l=1$ and 2 characters we get

$$k_1=\langle (2\cos\omega_i+1)/3\rangle=(2\langle\cos\omega_i\rangle+1)/3, \tag{13a}$$

$$k_2=\langle (4\cos^2\omega_i+2\cos\omega_i-1)/5\rangle$$

$$=(4\langle\cos^2\omega_i\rangle+2\langle\cos\omega_i\rangle-1)/5, \tag{13b}$$

so the only relevant features are the mean and the mean square of $\cos\omega_i$ over the trajectory. The fact that k_l is independent of the rotation axes $\{\mathbf{n}_i\}$ is intuitively reasonable, since the isotropy constraint does not distinguish any special directions. The spherical representation of SO(3) is thus very convenient, because all the configurations of a given concentric spherical surface will have the same contribution to the scaling factors.

Equations (13) constrain the set of possible scaling-factor combinations. To explore the allowed sequences, it is useful to introduce *spherical* trajectories or sequences, defined as scaling trajectories where the mean-square deviation of $\cos\omega$ vanishes, i.e., where ω is constant (but where $\mathbf{n}$ does

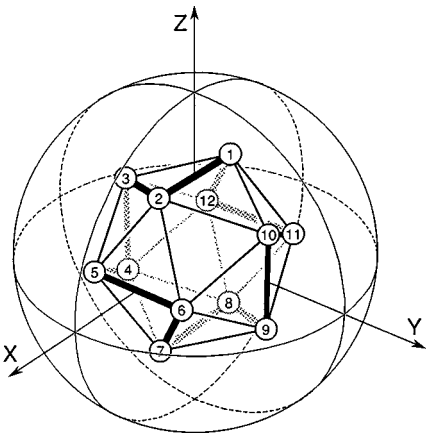

FIG. 3. An icosahedral sequence is represented by its configurations in the SO(3) group with the simplest C_3-symmetric path connecting them. The icosahedral symmetry ensures that the sequence accomplishes an isotropic scaling of all the spin couplings up to rank 2. The icosahedron has been embedded in the reference frame so as to have the C_2 symmetry axes along X, Y, and Z. The path corresponds to sequence (18) in the text and is C_3 symmetric around the magic $\langle 111\rangle$ direction. The pulse sequences associated with such trajectories are given in Table I for some specific values of the rotation angle ω.

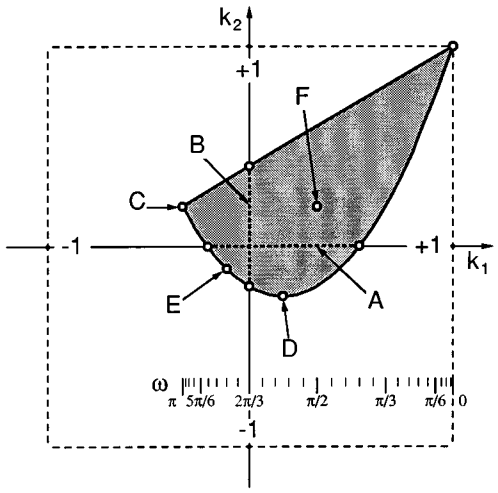

FIG. 4. The set of allowed combinations of first- and second-rank scaling factors for isotropic zero-field sequences. Scaling-factor combinations are represented by points in the (k_1,k_2) plane, and the grey area [given by Eqs. (16) in the text] is the set of allowed values. The sequences whose scaling combinations belong to the parabolic borderline are spherical trajectories associated with a fixed ω value given on the scale at the bottom. Some optimum combinations are of special interest: A: 2nd-rank decoupling with scaling of 1st-rank between $-(\sqrt{5}-1)/6$ and $(\sqrt{5}+1)/6$; B: 1st-rank decoupling with scaling of 2nd-rank between $-1/5$ and $2/5$; C: optimum time-reversal scaling for 1st-rank interactions, $k_1=-1/3$ (2nd-rank scaled by $k_2=1/5$); D: optimum time-reversal scaling for 2nd-rank interactions, $k_2=-1/4$ (1st-rank scaled by $k_1=1/6$); E: optimum scaling for time reversal of both 1st and 2nd-rank interactions, $k_1=k_2=-1/9$; F: zero-field in high-field (ZFHF) which can be regarded as the center of all the possible isotropic schemes (Refs. 13, 14), $k_1=1/3$ and $k_2=1/5$. The scaling combinations on the parabolic arc are generated by the icosahedral sequences listed in Table I.

change in order to have an isotropic result). An important property is that the effect of *an arbitrary scaling trajectory* is equivalent to a succession of spherical sequences used as building blocks. Indeed, the scaling factor for a given isotropic scheme, $\{R_i\}$, is determined by $\{\omega_i\}$ only. Therefore, an original sequence can be replaced by a succession of spherical sequences applied at the same ω values and for the same time intervals as defined by the $\{\omega_i\}$ distribution. In consequence, by analyzing the feasibility of spherical sequences, we shall be able to give the general rules limiting the set of allowed scaling factors.

IV. SPHERICAL, ICOSAHEDRAL AND TETRAHEDRAL SEQUENCES: THE SET OF ALLOWED SCALING FACTORS

Since the rotation angle ω is constant for spherical sequences, the Eq. (12b) becomes

$$\langle Y_{\lambda\mu}(\mathbf{n}_i)\rangle = 0 \quad \text{for any } 1\leqslant\lambda\leqslant 2l \quad \text{and } -\lambda\leqslant\mu\leqslant\lambda. \quad (14)$$

For specific values of ω, some generalized characters $\chi^l_\lambda(\omega)$ may vanish, thus reducing the set of λ values for which Eq. (14) has to hold. However, we shall restrict ourselves to the general case, because it is completely independent of ω. Furthermore, according to Eq. (14), any spherical sequence for a given value of l will be spherical for all values smaller than l as well. General solutions to Eq. (14) are well known[26,27] and have also been used in other NMR techniques such as MAS and WHH ($\lambda=2$), or DAS and DOR ($\lambda=2$ and 4).[5,6] For instance, it is possible to average out all spherical harmonics from $\lambda=1$ to 4, using icosahedral symmetry.[28] Equation (14) can thus be solved by selecting 12 rotation axes $\mathbf{n}_i$, with equal weights, and pointing towards the vertices of an icosahedron, as shown in Fig. 3. The corresponding δ-pulse sequences are called *icosahedral* spherical sequences.

Since Eq. (14) does not involve ω, spherical (for instance, icosahedral) trajectories are available for any value of ω. In the (k_1,k_2) plane, the set of scaling factors for spherical sequences is obtained by eliminating ω in Eqs. (13)

$$k_2=(9k_1^2-3k_1-1)/5, \quad (15)$$

where k_1 goes from $-1/3$ to 1 since $0\leqslant\omega\leqslant\pi$. The Eq. (15) describes a parabolic arc and, according to the last remarks of the previous section, the set of all allowed scaling factors is the concave side of the curve (the convex envelope) limited by the inequalities

$$-1/3\leqslant k_1\leqslant 1, \quad (16a)$$

$$(9k_1^2-3k_1-1)/5\leqslant k_2\leqslant(3k_1+2)/5. \quad (16b)$$

This area is shown in Fig. 4, and no other isotropic combinations are allowed. As a consequence, the isotropic scalings for first- and second-rank tensors are restricted to the following ranges:

$$-1/3\leqslant k_1\leqslant 1, \quad (17a)$$

$$-1/4\leqslant k_2\leqslant 1. \quad (17b)$$

The pulses required for icosahedral spherical sequences can be generated in many different ways according to the order in which the configurations are explored. To reduce the power requirements, it is simpler to explore the configura-

TABLE I. Lists of pulses (angles and axes) for the icosahedral isotropic sequences (18) and (19). The configurations explored by the sequences are labeled according to Fig. 3. Exact pulse parameters are listed in the third part of the table for some useful values of first- and second-rank scaling factors (also listed): decouplings ($k_l=0$), optimal time reversals ($k_l<0$ and minimum), and common time reversal of both ranks ($k_1=k_2<0$). The scaling factors and the pulses are deduced from the configuration parameter $\cos\omega$ according to Eqs. (13), (A5a), and (A6). The directions (u_2,ν_2,w_2), (u_4,ν_4,w_4) and (u'_5,v'_3,w'_3) are deduced from $(-\cos\theta,\sin\theta,0)$ by rotations, according to Eqs. (A7) and (A9). The direction $(u'_2,0,w'_2)=(-[(5-\sqrt{5})/10]^{1/2},0,-[(5+\sqrt{5})/10]^{1/2})$ is independent of ω, as explained in the Appendix. The second version of the sequence, Eq. (19), though less symmetric than Eq. (18), is more efficient for $\omega>124.54°$ as shown by the smaller total duration of the pulses (measured by the sum of the angle magnitudes).

Configuration		1	2	3	4	5	6	7	8	9	10	11	12	1
Pulse angle			α	α	α	α	α	α	α	α	α	α	α	α
Pulse	X		$-\cos\theta$	u_2	$\sin\theta$	u_4	0	w_2	$\cos\theta$	w_4	$\sin\theta$	ν_2	0	ν_4
axis	Y		$\sin\theta$	ν_2	0	ν_4	$-\cos\theta$	u_2	$\sin\theta$	u_4	0	w_2	$\cos\theta$	w_4
direction	Z		0	w_2	$\cos\theta$	w_4	$\sin\theta$	ν_2	0	ν_4	$-\cos\theta$	u_2	$\sin\theta$	u_4

Configuration		1	2	8	11	5	6	12	3	9	10	4	7	1
Pulse angle			α	β	α	β	α	β	α	β	α	β	α	β
Pulse	X		$-\cos\theta$	u'_2	u'_3	w'_2	0	w'_2	w'_3	0	$\sin\theta$	0	ν'_3	$-u'_2$
axis	Y		$\sin\theta$	0	ν'_3	$-u'_2$	$-\cos\theta$	u'_2	u'_3	w'_2	0	w'_2	w'_3	0
direction	Z		0	w'_2	w'_3	0	$\sin\theta$	0	ν'_3	$-u'_2$	$-\cos\theta$	u'_2	u'_3	w'_2

$\cos\omega$	$\cos\alpha$	$\cos\theta$	ω[b]	α[b]	θ[b]	k_1	k_2	Total angle[c]
$\frac{\sqrt{5}-1}{4}$	$\frac{\sqrt{5}-1}{4}$	$\sqrt{\frac{5+\sqrt{5}}{10}}$	72	72	31.7	$\frac{\sqrt{5}+1}{6}$	0	2.40
$-1/4$	$3\,\frac{\sqrt{5}-3}{16}$	$\sqrt{\frac{33-3\sqrt{5}}{58}}$	104.5	98.2	47.7	1/6	$-1/4$	3.27
$-1/2$	$\frac{3\sqrt{5}-13}{20}$	$\sqrt{\frac{25-3\sqrt{5}}{58}}$	120	108.3	55.8	0	$-1/5$	3.61
$-2/3$	$\frac{\sqrt{5}-6}{9}$	$\sqrt{\frac{7-\sqrt{5}}{22}}$	131.8	114.7	62.3	$-1/9$	$-1/9$	3.82(3.52)
$-\frac{\sqrt{5}+1}{4}$	$-1/2$	$\sqrt{\frac{3-\sqrt{5}}{6}}$	144	120	69.1	$-\frac{\sqrt{5}-1}{6}$	0	4.00(3.20)
-1	$-3/5$	0	180	126.9	90	$-1/3$	1/5	4.23(2.11)

[a]Where $\beta=2(\pi-\omega)$.
[b]In degrees.
[c]In turns per cycle for the first version of the sequence; for $\omega>120°$ the numbers in parenthesis refer to the second version of the sequence.

tions by joining closest neighbors as in Fig. 3, so all the pulses have the same length α. Furthermore, if the three coordinate axes are chosen along C_2 symmetry axes of the icosahedron, the configuration path can be designed so as to display a C_3 symmetry along the magic $\langle 111\rangle$ direction. This makes it possible to deduce the pulses from each other by cyclic permutations of the three coordinates. In this way, the icosahedral sequences can always be written according to the pattern

$$\omega-([(\tau/2-\alpha_i-\tau/2)_{i=1,4}]_{3\text{c.c.}})_n-(-\omega), \tag{18}$$

where 3 c.c. stands for the repetition, with cyclic permutations of the coordinates, of the four pulses α_i. Icosahedral sequences, like all other spherical trajectories, require that the initial and final pulses are applied in order to connect the initial state at $\omega=0$, with the configurations at the selected nonzero ω. Analytical expressions for the α_i pulses as a function of ω are given in the Appendix, and some special combinations of scaling factors are listed in Table I; they are decoupling and optimal time reversal, for first- and second-rank tensors.

Sequences such as Eq. (18) are not necessarily the most efficient because the associated configurations are distributed in a folded space [the SO(3) group]: In the folded structure of SO(3), two opposite points on the π sphere represent the same rotations. The closest neighbors to a given vertex are not always limited to the five next vertices of the icosahedron, but they can also include the opposite vertex. As shown in the Appendix, when ω is above 124.54° [$\cos\omega=-(4+\sqrt{5})/11$], the icosahedral distribution of configurations can thus be explored according to the more efficient pattern

$$\omega-([\tau/2-\alpha_1-\tau-2(\pi-\omega)_2-\tau-\alpha_3-\tau$$
$$-2(\pi-\omega)_4-\tau/2]_{3\text{c.c.}})_n-(-\omega), \tag{19}$$

in which the C_3 symmetry is preserved. The limiting case $\omega=\pi$ is especially important, because the twelve vertices of the icosahedron are then reduced to six. Detailed pulse parameters for some special values of ω are also given in Table I.

Compared to the previously available coherent schemes, the icosahedral sequences introduce significant improvements for many applications:

(1) Global time reversal (ranks 1 and 2). The optimum scaling is $(k_1,k_2)=(-1/9,-1/9)$ with an icosahedral sequence. The previous limit was $(-1/11,-1/11)$ in time-reversal sequences that could be deduced from some decoupling schemes, by removing the identity configurations they contained (a similar procedure exists in HF-NMR between the WHH and the magic sandwich sequences).

(2) Rank-selective time reversal. For the first-rank interactions, the theoretical optimum of $k_I=-1/3$ was already obtained from the previous decoupling scheme,[18] but the present icosahedral sequences are also isotropic for second-rank interactions. For the second-rank interactions, the icosahedral trajectories provide the optimum time-reversal scaling at $k_2=-1/4$, exceeding the previous value of $-1/8$ (obtained again from a decoupling scheme, the discrete zero-field version of MAS[18]).

(3) Rank-selective decoupling. A scheme to decouple both first-and second-rank tensors was available,[18] but icosahedral sequences make it now possible to build isotropic, rank-selective decoupling schemes. When decoupling the first-rank interactions, the second-rank tensors can be scaled between $-1/5$ and $2/5$, whereas for second-rank decoupling, the first-rank tensors are scaled between $-(\sqrt{5}-1)/6$ and $(\sqrt{5}+1)/6$.

It should be noted that except for the special values of $\omega=2\pi/5$ or $4\pi/5$, where the configurations belong to the icosahedral group, the angles and axes of the pulses are not associated in any simple way with any known subgroup of SO(3), even for optimum combinations of scaling factors, like $(-1/3,1/5)$ or $(1/6,-1/4)$. Although many high-field sequences generally involve group rotations as pulses (usually $\pi/2$ along X and Y), this is not a relevant symmetry of the process. When designing a coherent process, the various constraints (for example, the isotropy conditions in the present case) can be translated into group symmetrical properties of the configuration trajectory, but this does not imply that the configuration trajectory is the group itself, just as a polytope in the Euclidean space is not equivalent to its symmetry group.

So far we have only considered icosahedral spherical sequences, since almost all the local interactions behave as second-rank tensors. If only first-rank tensors are involved (due to residual magnetic fields, for instance), Eq. (14) has to hold for $\lambda\leqslant 2$ instead of 4. At constant ω, this is accomplished by means of a tetrahedral distribution of four directions $\mathbf{n}_i$, so the pulse sequences, which are deduced by a procedure similar to the icosahedral case, are considerably simpler. Sequences for time reversal and decoupling are of particular importance. For decoupling, the configurations happen to be at $\omega=2\pi/3$, and form the $2\pi/3$ class of the tetrahedral subgroup in SO(3), so the sequence involves only π pulses along the X and Y axes

$$(2\pi/3)_M-(\tau/2-\pi_X-\tau-\pi_Y-\tau-\pi_X-\tau-\pi_Y-\tau/2)_n -(-2\pi/3)_M. \tag{20}$$

where the index M labels pulses applied along the magic direction, $\langle 111\rangle$. This sequence was already deduced previously.[18] For optimum time reversal, it should be noticed that $\omega=\pi$, so the configurations of opposite directions are identical. A distribution of tetrahedral symmetry can thus be obtained with only three points on the X, Y, and Z axes, corresponding to the centers of the six edges of a tetrahedron (this set actually has a higher, octahedral symmetry). Again, the set of configurations is found to be the $\omega=\pi$ class of the tetrahedral subgroup in SO(3), and the resulting sequence consists of π pulses only

$$\pi_X-(\tau/2-\pi_Y-\tau-\pi_X-\tau-\pi_Z-\tau/2)_n-\pi_X. \tag{21}$$

V. DECOUPLING SEQUENCES

As we have already mentioned in Sec. II, the symmetry properties of decoupling schemes are wider than those of isotropic schemes in general [see Eq. (5)]. Decoupling sequences can be generated as special cases of isotropic sequences, but other trajectories can be designed which result from the SO(3)×SO(3) symmetry. In the same way that Eq. (8) was expanded into irreducible representations of SO(3) for the general isotropic case, we now expand it into irreducible representations of SO(3)×SO(3), with $k_l=0$. Instead of the adjoint representation defined by Eq. (10), we have the product representation

$$M_{m'm}\rightarrow(\mathbf{U}\times\mathbf{V})(M_{m'm})=\sum_{nn'} D^l_{m'n}(U)M_{n'n}D^l_{nm}(V), \tag{22}$$

whose irreducible representations are known to be the tensor products of the SO(3) irreducible representations, labeled as $l\otimes l'$.[22] For the left-hand product of the matrix M by rotation U in Eq. (22), constant-m columns of the $M_{m'm}$ matrix transform as a $(2l+1)$-dimensional vectors in the lth-order irreducible representations. We also have a similar property for the right-hand product on constant-m' rows. So Eq. (8) is already in its irreducible tensor form, and only one representation is involved, $l\otimes l$. In contrast to the general isotropic case, the completely invariant representation, here $0\otimes 0$, is not present. This is consistent with the fact that we are dealing with a decoupling trajectory.

The identification of the appropriate symmetry groups is a useful step in the solution of nonlinear (though algebraic) problems like Eq. (8). An important and extensively explored example is the quadrature on a sphere in three-dimensional Euclidean space:[26,27] We ask how to find a set of discrete points $\mathbf{n}_i$ on a sphere, such that the average of any spherical harmonic over $\{\mathbf{n}_i\}$ vanishes, up to some given l value [we already came across this problem in Eq. (14)]. Since any set $\{R(\mathbf{n}_i)\}$ is also a solution if $\{\mathbf{n}_i\}$ is a solution, the invariance group is SO(3) again. To generate a discrete set $\{\mathbf{n}_i\}$ (or $\{R_i\}$ in our problem), one can start from an initial orientation $\mathbf{n}_0$, called the ''seed,'' and apply a discrete subgroup of SO(3), G.[26] In this way we build a set, called an ''orbit,'' as $\{\mathbf{n}_i\}=\{g(\mathbf{n}_0)\}_{g\in G}$. The distribution of points is then strongly constrained, but simple group-theoretical arguments can tell us if Eq. (14) is fulfilled.[26] For instance, whatever the seed, the tetrahedral, cubic, and icosahedral groups are known to

cancel spherical harmonics up to $l=2$, 3, and 4, respectively. These limiting values can be increased by a proper choice of $\mathbf{n}_0$ with respect to the symmetry axes, or by combining two or more seeds, and analytical solutions can be found in this way for maximum l values of up to 17.[27]

The group-theoretical approach to solve this type of problem generally consists of three main steps: Identifying the invariance group, selecting some discrete subgroup which already solves most of the equations, and choosing an appropriate seed to fulfill the remaining conditions. For instance, when solving Eq. (8) for isotropic scaling in Sec. IV, we selected a configuration at some given ω, and applied the icosahedral group to generate a solution. Incidentally, it should be noted that the icosahedral group contains 60 elements, but the icosahedral sequences (like those we listed in Table I) contain only 12 configurations, because the seed was chosen on a C_5 axis to obtain a smaller orbit. This specific solution using the 12 vertices of the icosahedron can also be considered to be generated by the *tetrahedral* group, starting from a particular seed to cancel the spherical harmonics at $l=3$ and 4 that are not normally averaged out by the smaller group.

The symmetry arguments can also be applied to our decoupling problem, $k_l=0$, which can be seen as a quadrature over the SO(3) space (instead of over the usual sphere in three-dimensional Euclidean space). Accordingly, solutions we search for are configuration sets defined by orbits generated from a subgroup of SO(3)×SO(3) acting on a seed R_0. If the subgroup is of the type $G\times H$, where G and H are subgroups of SO(3), then the configurations are $\{R_i\}=\{g\cdot R_0\cdot h\}_{(g,h)\in G\times H}$. If we use the $C_{3Z}\times C_{3Z}$ subgroup of SO(3)×SO(3), Eq. (8) gives for $l=2$

$$\langle D^2_{mm'}(R_i)\rangle=(1/9)\sum_{\alpha,\gamma=0,\pm 2\pi/3} e^{im\alpha}D^2_{mm'}(R_0)e^{im'\gamma}$$
$$=\delta_{0m}\delta_{0m'}D^2_{00}(R_0)=0. \tag{23}$$

Decoupling can thus be achieved if we select the seed R_0 to cancel the remaining element, D^2_{00}, for instance using a rotation by $\beta=\theta_m$ (the magic angle, $\cos^2\theta_m=1/3$) around the Y axis. With this trajectory the first-rank tensors are neither decoupled nor isotropically scaled, because

$$\langle D^1_{mm'}(R_i)\rangle=\delta_{0m}\delta_{0m'}D^1_{00}(R_0)=\delta_{0m}\delta_{0m'}/3^{1/2}\neq 0. \tag{24}$$

As we shall see in the next section, this trajectory, which we term ''discrete MAS,'' is the discrete zero-field analog of the usual, high-field MAS and WHH sequences. A similar trajectory to decouple second-rank interactions was also explored within the more restrictive framework of the cubic group.[18] In the present formalism, it can be generated by the same seed R_0, but using the subgroup $C_{4Z}\times C_{3Z}$.

First-rank tensors can be decoupled by applying four-pulse sequences based on the $C_{2Z}\times C_{2Z}$ group, and using a rotation by $\beta=\pi/2$ around Y as a seed. In this particular case, the set of configurations can be identified with the dihedral group D_2 (identity and three π rotations along X, Y, and Z), and it can also be generated by the subgroup $D_2\times\{I\}$, with the identity as a seed. Aside from a global $2\pi/3$ rotation of the configurations around the magic $\langle 111\rangle$ direction, this trajectory is also identical to the $l=1$ tetrahedral decoupling sequence (20) described in Sec. IV. As shown by the discrete-MAS case, however, it is not always possible to reduce a decoupling sequence to a special case of isotropic scaling.

Another interesting case arises in decoupling both first- and second-rank tensors. This can be done by a 13-pulse combination of spherical sequences, for instance, at $(k_1,k_2)=(-1/9,-1/9)$ and (1,1) (see Fig. 4). But, as already shown,[18] it can also be performed regardless of the seed by the subgroup $T\times\{I\}$, where T is the tetrahedral group. Indeed, the tetrahedral group is known to cancel *all* of the $l=1$ and 2 tensors,[28] so each constant m' column of the Wigner matrix in Eq. (8) is averaged out. Now, in the SO(3) spherical representation, this set of configurations has 1, 8, and 3 elements on spheres, respectively, at $\omega=0$, $2\pi/3$, and π, so it cannot be reduced to a combination of spherical isotropic sequences. By a proper selection of the seed, the tetrahedral sequence can also be generated by the $D_2\times C_{3Z}$ subgroup.

At this point we can compare, on a qualitative basis, the efficiency of the various sequences we have discussed so far. If we disregard the pulse lengths in the first approximation, the efficiency is given by the number of configurations involved in the averaging schemes. For $l=1$ and 2, Eq. (8) consists of 9 and 25 conditions, respectively, to be matched with a set of $3N$ parameters (we assume equal weights on all of the N configurations). We can thus expect that 3 or 9 configurations will be needed respectively, and up to 12 configurations in the case of a sequence that is isotropic for both $l=1$ and 2. In view of this, the discrete-MAS and icosahedral sequences can be considered as the optimum, whereas the tetrahedral sequences for first-rank tensors appear less efficient.

VI. HIGH FIELD ISOTROPIC SCHEMES

The relationships between high-field and zero-field coherent schemes were previously pointed out for decoupling sequences,[18] and for the zero-field in high-field NMR technique (ZFHF)[14] mentioned in Sec. I. These two classes of high-field methods can be seen as isotropic scalings processes, and in the present section we analyze them as zero-field trajectories according to the general theory of isotropic scaling.

The translation of high-field schemes into zero field involves two main steps. First, any NMR experiment can be viewed, theoretically, as a zero-field process; the static magnetic field in HF-NMR is a ''very long'' dc pulse, of many times 2π, and any high-field coherent technique is then a ''windowless sequence.'' MAS and ZFHF are thus zero-field decoupling, and zero-field isotropic scaling schemes, respectively. Second, any physical reorientation of the sample in a zero field can be mimicked by an opposite motion of the spins with a fixed sample. This is easily seen for all the local interactions that are not field dependent (like the dipolar, quadrupolar and J couplings), because the corresponding Hamiltonians for a rotated sample can be transformed according to

$$H=\sum_m (-1)^m A_{l,-m}(R(\Omega))T_{lm}$$

$$=\sum_{mm'} (-1)^m D^l_{-m',-m}(R)A_{l,-m'}(\Omega)T_{lm}$$

$$=\sum_{mm'} (-1)^{m'} A_{l,-m'}(\Omega)D^l_{m,m'}(R^{-1})T_{lm}$$

$$=\sum_m (-1)^m A_{l,-m}(\Omega)R^{-1}(T_{lm}), \tag{25}$$

(where we have used the symmetries of the Wigner matrices[25]). This result can also be understood in terms of reference frames: an active rotation of the sample is equivalent to the opposite passive rotation of the laboratory frame which defines the spin-quantization axes.

When considering high-field coherent processes, one may think that the above equivalence of sample and spin motions is not valid anymore because the interactions are truncated. Indeed, the truncated Hamiltonian of the coupling becomes

$$H=A_{l0}(\Omega)T_{l0}, \tag{26}$$

and a sample rotation cannot be transformed into a spin rotation just as it could in Eq. (25). However, if we consider the Zeeman field as a part of the coherent process (as a strong $2k\pi$ pulse), we have to *rotate it together with the spins* in order to properly imitate the sample motion. In the configuration space SO(3) the Zeeman coupling generates a loop trajectory, and a rotation of the spins or the lattice is actually represented by a rotation of this loop. The sample motion can thus be replaced by a reorientation of both the main magnetic field and the spins around the fixed sample.

An illustrative example is provided by the MAS trajectory in a high field.[3,2,7] In MAS, decoupling of second-rank interactions, like dipolar couplings, is achieved by spinning the sample around an axis at the magic angle with respect to the magnetic field. The corresponding zero-field version consists of rotating the magnetic field around a magic cone, as shown in Fig. 5. The motion must be adiabatic, just as in the standard high-field MAS. In a nonadiabatic version of MAS, magic hopping,[29] the sample is reoriented by discrete jumps of $2\pi/3$ around the magic direction. This can also be translated to a zero-field version, by applying the field for $2n\pi$ periods along the X, Y and Z directions, and adding $2\pi/3$ δ pulses along the magic direction in order to have the spins accompany the field trajectory (Fig. 5). A pure δ-pulse version can be generated when the long $2n\pi$ pulses are replaced by three $2\pi/3$ pulses (since they generate, in the first order, the same truncation of the second-rank interactions).

Second-rank interactions can also be averaged in a high field using rf irradiation. In WHH, the spins are nutated along the X, Y, and Z directions by rf pulses.[4,2,7] The Lee–Goldburg experiment is a continuous version of WHH, where an off-resonance irradiation causes the spins to precess around the magic $\langle 111\rangle$ axis $\mathbf{M}$.[7,30] Both of these schemes can be viewed as zero-field processes. The zero-field version of WHH, shown in Fig. 5, is similar to that of magic hopping, although the $2n\pi$ pulses are always applied

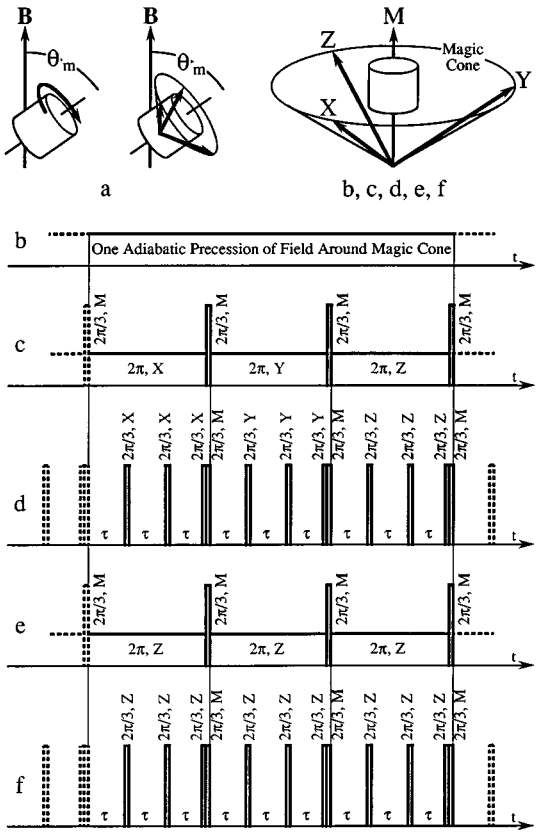

FIG. 5. Construction of the δ-pulse, zero-field versions of some common high-field trajectories that decouple second-rank tensors [MAS (Ref. 3), WHH (Ref. 4) and magic hopping (Ref. 29)]. The sample rotation in a fixed high magnetic field, (a), is transformed into a motion of the magnetic field around a fixed sample: either adiabatically for MAS, (b), or by sudden reorientations combined with pulses for magic hopping, (c). The WHH sequence is readily transformed as in (e), since it does not involve any sample motion. All these sequences can be transformed into their δ-pulse equivalents as in (d) for MAS and magic hopping or (f) for WHH, since the truncation effect of second-rank interactions by a static field can be obtained with three $2\pi/3$ rotations. These discrete MAS sequences are equivalent and consist of nine configurations generated by the discrete $C_3\times C_3$ subgroup of SO(3)×SO(3) (see Sec. V). They cannot be reduced to spherical sequences.

along the same direction Z. When comparing the pure δ-pulse versions of the WHH and magic-hopping experiments (Fig. 5), we obtain the same sets of nine configurations, although the path exploring them is different. For instance, the configurations in the discrete WHH and magic-hopping cases can be written as

$$R_{\mathrm{WHH}}(i,j)=R(2i\pi/3,\mathbf{M})\cdot I\cdot R(2j\pi/3,\mathbf{Z}), \tag{27a}$$

$$R_{\mathrm{MH}}(i,j)=R(2i\pi/3,\mathbf{M})\cdot I\cdot R(2j\pi/3,\mathbf{ZYX}(i)), \tag{27b}$$

where i and j are integer indices running from -1 to 1, $R(\alpha,\mathbf{n})$ denotes the configuration given by rotation α around axis $\mathbf{n}$, and $\mathbf{ZYX}(i)$ is the axis $\mathbf{Z}$, $\mathbf{Y}$, or $\mathbf{X}$ depending on the value of i. Equation (27b) can be rewritten as:

$$R_{\mathrm{MH}}(i,j)=R(2i\pi/3,\mathbf{M})\cdot R(2j\pi/3,\mathbf{ZYX}(i))$$
$$\times R(2i\pi/3,-\mathbf{M})\cdot R(2i\pi/3,\mathbf{M}),$$
$$=R(2j\pi/3,\mathbf{Z})\cdot R(2i\pi/3,\mathbf{M}), \tag{28}$$

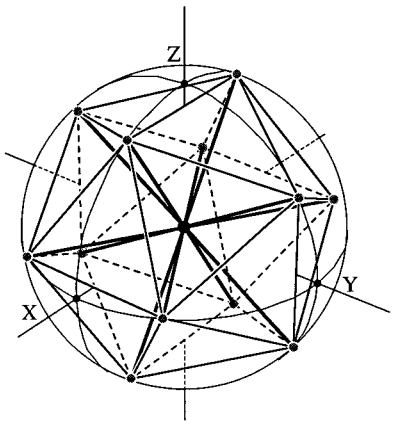

FIG. 6. The configuration trajectory of the simplest zero-field in high-field NMR experiment, or ZFHF (Ref. 14), consists of six straight lines along the C_5 axes of an icosahedron in the SO(3) space (thick lines). In fact, the lines become loops because of the folded structure of SO(3). ZFHF sequence isotropically scales first- and second-rank interactions by 1/3 and 1/5, respectively. This generic sequence provides an isotropic path connecting all the concentric icosahedral sets of configurations. For instance, by introducing stops at the spheres defined by $\omega=0$ and $\omega=\pi$ (large points at the center and the vertices of the icosahedron), the rank-selective decoupling sequence (35) in the text can be generated. The icosahedral symmetry ensures the isotropic character of the sequence, even with finite pulses.

which is now clearly identical to Eq. (27a) by exchanging the rotation axes, **M** and **Z**, and the indices i and j. These arguments show how all the high-field decoupling experiments (like MAS, WHH, and magic hopping) display the same general $C_\infty\times C_n$ symmetry (which can, eventually, be discretized into $C_3\times C_3$). The main Zeeman interaction generates an averaging through the C_∞ group, and the decoupling process is completed by a spin or lattice motion through C_3 (WHH, magic hopping) or C_∞ (MAS).

As shown in the previous sections, isotropic scaling schemes cannot be generated using $C_\infty\times C_n$ symmetries. The isotropic scaling schemes in a high field, such as ZFHF, are thus more complex than the decoupling techniques. The simplest ZFHF trajectory can be described as a windowless zero-field sequence, involving only six 2π pulses along the C_5 axes of an icosahedron.[14] This corresponds to straight radial paths in the SO(3) space, as shown in Fig. 6, and the icosahedral symmetry yields isotropic scalings for first- and second-rank couplings, according to the arguments of Sec. IV. The scaling factors are just the averages over $\omega=0$ to π in Eqs. (13), and give $(k_1,k_2)=(1/3,1/5)$ as plotted in Fig. 4. From this sequence, where the magnetic field is always applied, sequences in a high *static* field were designed[14] by replacing the magnetic-field reorientation by a sample motion synchronized with the proper pulse sequence, according to the general principles of equivalence between high- and zero-field schemes. For practical purposes, however, the sequences effectively used in a high-field are not based on the icosahedral scheme;[14] still this approach shows that isotropic scaling is indeed completely achievable in a high field. The icosahedral six-pulse sequence still plays a central role in pulse compensation of zero-field sequences, as shown in the next section.

The general question of high-field isotropic schemes can be discussed within the theoretical framework of zero-field isotropic scaling. In high-field schemes, both sample rotations and spin irradiations are adiabatic compared to the main Zeeman frequency, ω_Z, and this translates in the SO(3) configuration space by a succession of slowly rotating 2π loops. The configurations along such a path are given by

$$R^{-1}_{\text{lattice}}(t)\cdot R(\omega_Z t,\mathbf{Z})\cdot R_{\text{spins}}(t), \tag{29}$$

where the time modulation of the spin and lattice parts is much slower than the Zeeman frequency. This adiabatic approximation makes it legitimate to average independently over $\alpha=\omega_Z t$ and over the lattice and spin configurations, and the isotropic conditions become

$$\left\langle \left\langle \sum_n D^l_{m'n}(R^{-1}_{Li})e^{in\alpha}D^l_{nm}(R_{Si}) \right\rangle_\alpha \right\rangle_i$$

$$=\langle D^l_{0m'*}(R_{Li})D^l_{0m}(R_{Si})\rangle_i=k_l\delta_{m'm}. \tag{30}$$

This equation, an analog to Eq. (8), was already explored,[14] and we shall only give the corresponding area of allowed scaling factors. By taking the trace of Eq. (30), we obtain the scaling factors as

$$k_l=\langle D^l_{00}(R_{Si}\cdot R^{-1}_{Li})\rangle_i/(2l+1), \tag{31}$$

so they depend upon the Legendre polynomials of $\cos\beta_i$ only, where β_i is the second Euler angle of the combined spin and lattice rotation $R_{Si}\cdot R^{-1}_{Li}$. For first- and second-rank interactions this gives

$$k_1=\langle\cos\,\beta_i/3\rangle_i, \tag{32a}$$

$$k_2=\langle(3\,\cos^2\,\beta_i-1)/10\rangle_i. \tag{32b}$$

Just as in the general isotropic case, it can be proved that any scheme at constant β_i can be built using the icosahedral symmetry again. The set of allowed scaling factors in a high field is thus defined by

$$-1/3\leqslant k_1\leqslant 1/3, \tag{33a}$$

$$(27k_1^2-1)/10\leqslant k_2\leqslant 1/5, \tag{33b}$$

which is shown in the (k_1,k_2) plane in Fig. 7. In any case, the scaling factors are limited by

$$-1/3\leqslant k_1\leqslant 1/3, \tag{34a}$$

$$-1/10\leqslant k_2\leqslant 1/5. \tag{34b}$$

In practical situations, the sample motion is almost always restricted to a steady, high-speed rotation around a single, fixed axis. The set of allowed scaling factors is then reduced even further, and many important properties of optimal isotropic trajectories are lost. For instance, isotropic behavior may hold for second-rank couplings, but not for first-rank ones. The trajectories also lose their icosahedral symmetry.

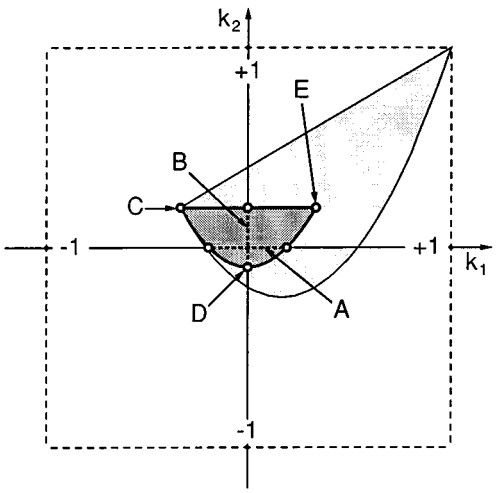

FIG. 7. The set of allowed combinations of first- and second-rank scaling factors for isotropic high-field sequences. As in Fig. 4, scaling factor combinations are represented by points in the (k_1,k_2) plane, and the dark-grey area [given by Eqs. (33)] is the set of allowed values. For comparison, the set of allowed scaling factors for unrestricted isotropic schemes is given in light grey (see Fig. 4). The outlined points are the optimum combinations of scaling factors, for decoupling and time reversal: A: 2nd-rank decoupling, 1st-rank scaling between $-1/(3\sqrt{3})$ and $1/(3\sqrt{3})$; B: 1st-rank decoupling, 2nd-rank scaling between $-1/10$ and $1/5$; C: optimum time-reversal scaling for 1st-rank interactions, $k_1=-1/3$, 2nd-rank scaled by $k_2=1/5$; D: optimum time-reversal scaling for 2nd-rank interactions, $k_2=-1/10$, 1st-rank decoupled; F: the simplest zero-field in high-field NMR sequence, or ZFHF (Ref. 14), gives the maximum scaling factors for first- and second-rank interactions, with $k_1=1/3$ and $k_2=1/5$.

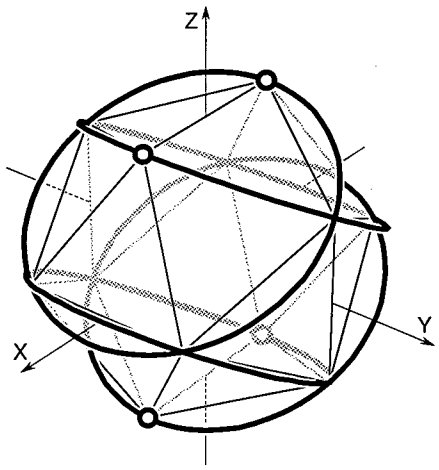

FIG. 8. The configuration trajectory for a spherical windowless scaling sequence based on an icosahedral set of configurations in SO(3) (ω has an arbitrary fixed value and the outline of the π sphere is not shown). The lines are obtained by rotating the icosahedron in Fig. 3 around two C_5 axes. Each point on the curve can be associated with eleven other points to form an icosahedron. Since this trajectory is a loop joining all the nodes, which are evenly branched, it can be fully explored in just one run. In order to obtain an isotropic scaling, the circles are explored at a constant speed, and the sequence must stop at each of the four outlined points for the same amount of time otherwise needed to explore a complete circle.

VII. FINITE PULSE COMPENSATIONS: AN EXPERIMENTAL EXAMPLE USING THE ZFHF TRAJECTORY

Experimentally, the finite length of the pulses is the most important limiting factor for coherent averaging schemes in systems displaying strong couplings, such as dipole–dipole interactions between protons in solid-state samples. It is thus worthwhile to analyze more carefully the possibilities of icosahedral sequences in that respect. By pulse compensation we mean the removal of any residual anisotropic interaction due to the finite length of the pulses, although changes (hopefully small) of the isotropic scaling factors are tolerated. We shall review three main possibilities: icosahedral pulse compensations, spherical windowless trajectories, and the zero-field-in-high-field path. We shall also give an experimental example of this last possibility.

The configuration trajectory for an icosahedral sequence with finite pulses does not display an overall icosahedral symmetry, as shown in Fig. 3, so it is not compensated for the pulse lengths. A theoretically simple solution to the problem is to restore the icosahedral symmetry by using pulses corresponding to all of the 30 different edges of the icosahedron. However, since each vertex is connected to the others by an odd number of edges (five), the whole path would need to have at least 60 pulses. It should also be noted that during the pulses the explored configurations are not confined to a constant ω sphere, because they are on the shortest path from one vertex to the next. In any case then, the scaling factors of the pulse-length compensated sequences will be slightly different from those of the original δ-pulse versions.

Based on the icosahedral distribution of configurations, it is also possible to design some spherical windowless sequences. For this, it is just necessary to connect all the vertices by a single path, in such a way that, for each point on the trajectory, there are eleven other points on the trajectory to form an icosahedron. This can be simply done by reorienting an icosahedron while following its vertices, for instance, using 2π rotations around two of the C_5 axes, as in Fig. 8. The whole path can be fully traced just once by a continuous trajectory since there is an even number of lines connected to any vertex. The sequence can be shown to consist of successive periods of constant-speed precessions of the field around various fixed cones, with matching conditions between the cone angles, the precession speed, and the field strength.

Although these methods are conceptually simple and efficient as far as scaling factors are concerned, the corresponding magnetic-field trajectories are rather involved. The magnetic fields are generated by coils wound around the sample, with their appropriate power supplies controlled from a pulse programmer, and the simplest design involves three coils to create the orthogonal coordinates of the field. With this kind of experimental setup, it is rather difficult to calibrate the very general pulse directions and angles needed in icosahedral sequences, especially when about 60 of them are threaded and expected to yield no final rotation. For the windowless trajectories the calibration procedure would be even more tedious, given all the specific synchronization conditions between the magnitude, precession speed and precession angle of the field.

A much simpler path, joining the vertices while preserv-

ing the icosahedral symmetry, is provided by the zero-field in high-field trajectory (ZFHF),[14] introduced in the previous section. Since it consists of six 2π pulses along the vertex directions of an icosahedron, the ZFHF trajectory connects all the vertices of icosahedra lying on all the possible spheres of constant ω, as shown in Fig. 6. Owing to its icosahedral structure, the trajectory provides paths from one vertex to the next, via the identity point, that are intrinsically compensated for finite pulse lengths. Any combination of scaling factors can thus be generated by appropriately splitting the 2π pulses and adding free-evolution periods (see Fig. 6). The pulses contribute to the scaling factors by 1/3 and 1/5 for first- and second-rank tensors, respectively, so the ZFHF trajectory can be considered as a central point in the set of allowed scaling factors (see Fig. 4), i.e., it is obtained by averaging the spherical sequences over all possible ω values with a constant weight. Furthermore, as already mentioned in Sec. IV, any spherical or near-spherical sequence involves initial and final pulses from identity to some configuration at the selected ω; to compensate for the finite lengths of these pulses, it would thus be necessary, in general, to add supplementary paths to the identity, a feature already taken into account by the ZFHF trajectory.

We carried out an experiment using a ZFHF-based sequence to average out first-rank tensors while preserving scaled second-rank tensors. This technique can be useful in applications where the residual magnetic fields cannot be properly compensated and distort the zero-field spectrum generated by local interactions. We used a 12-π-pulses sequence according to the general scheme described above, stopping at the $\omega=0$ and $\omega=\pi$ configurations (as shown in Fig. 6) to generate the highest possible scaling factor for the second-rank tensors while still decoupling the first rank. The sequence can thus be written as

$$[(\tau-\pi_i-3\tau-2\tau'-\pi_i)_{i=1,6}]_n, \tag{35}$$

where τ' is the length of the π pulses, and i labels the six icosahedral C_5 axes. This sequence is compensated for finite pulse lengths and the second-rank scaling factor is

$$k_2=(2\tau+\tau')/5(\tau+\tau'), \tag{36}$$

which is always between 1/5 and 2/5. The sequence was applied to the proton spins of CH_2Cl_2 dissolved in a disordered smectic-E liquid crystal (5%–10% wt in a 50%–50% wt mixture of 4-*n*-butyloxybenzylidene-4′-*n*-octylaniline and 4-*n*-octyloxy-4′-*n*-cyanobiphenyl). The pure zero-field spectrum of this sample was already reported[31] and, as shown in Fig. 9(a), it consists of three transitions at 0.2, 1.4, and 1.6 kHz, arising from the residual anisotropic dipolar coupling between the two protons. When a small residual field is present, the lines broaden and a sharp parasitic peak at the zero frequency appears [see Fig. 9(a)]. Eventually, for residual fields strong enough, the transitions cannot be distinguished any more and only the central peak remains. This is shown in the spectrum of Fig. 9(b), obtained as the zero-field spectrum in Fig. 9(a), but with a stronger residual field applied by deliberately setting the zero-field shimming coils in our spectrometer far from the optimal values ($\approx 100\times10^{-7}$ T along the Y axis and a gradient of

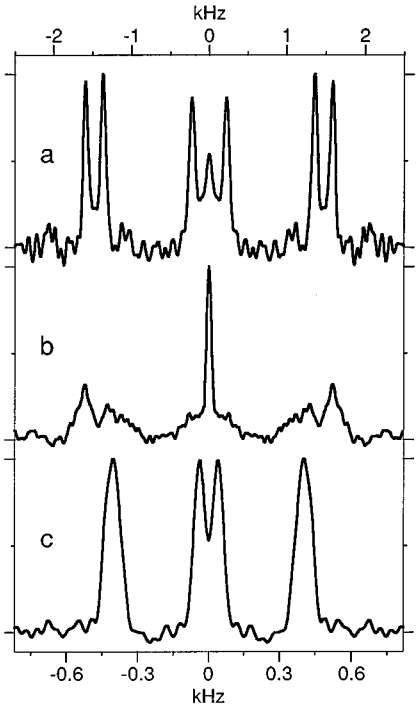

FIG. 9. Proton zero-field spectra of CH_2Cl_2 dissolved in a randomly oriented smectic-*E* liquid crystal: (a) with optimal shimming conditions of the zero-field region of the spectrometer; (b) with the presence of an inhomogeneous, randomly oriented, residual magnetic field in the 0.2×10^{-4} T range; (c) in the same conditions as (b), but recorded using a rank-selective icosahedral sequence that decouples first-rank couplings but isotropically scales second-rank interactions by about 0.33. The residual fields in the spectrometer distort the zero-field spectrum: at low fields a parasitic peak at zero frequency appears, and at higher fields the structure of the whole zero-field spectrum is obscured. By using the decoupling sequence, some of the original structure of the zero-field spectrum is retrieved and the central peak is suppressed. Pulse imperfections and nonvanishing high-order terms in the averaged couplings introduce distortions, which make it difficult to resolve the high-frequency lines.

$\approx 50\times10^{-7}$ T along Z over the sample height). With the same inhomogeneous residual field, but using the icosahedral $l=1$ decoupling sequence (35) during the free evolution of the system, the spectrum recovers most of its usual zero-field features, as shown in Fig. 9(c), although all the frequencies are scaled by about 1/3. The residual central peak of the usual zero-field spectrum, due to uncompensated residual fields, is fully removed, although the third- and higher-order terms in the average Hamiltonian, the pulse transients, and the eddy currents induce a broadening and a distortion of the spectrum. The expected 200 Hz fine structure of the transitions around 1.5 kHz is thus obscured by poor resolution.

The experiment was carried out on a modified version of our zero-field spectrometer.[32] The sample polarization was prepared and monitored using field cycling with a sample-shuttling system,[11,32] and the zero-field evolution was initiated and terminated by the sudden switching of a magnetic field (along the main Z axis) stronger than the local interactions.[11] Three class A, dc to 1 MHz, 2 kW amplifiers were interfaced to the 0.1 μs resolution pulse programmer via 12-bit digital-to-analog converters. They provided up to 75×10^{-4} T in three orthogonal coils, X, Y, and Z, around the

zero-field region of the spectrometer. The homogeneity and the orthogonality of the coils over the sample (0.6 mm diameter and 0.7 mm height) were better than 0.5%. Using nutation experiments on a water sample, the amplitudes of the three coordinates of the icosahedral π pulses were adjusted from their theoretical values to account for the nonlinearities, imbalances and transient effects in the three power amplifiers. Pulse transients are due not only to the finite rising and falling times of the currents in the coils, but also to the differences in rising and falling times if the pulses are not only along X, Y, or Z. We refer to the latter effects as orientation transients, which are analogous to phase transients in high-field NMR.[7] The nutation adjustment ensured that, even after a train of many hundred cycles, the sequence did not generate any residual rotations that would have distorted the spectrum in the form of an effective Zeeman coupling. Symmetric cycles with opposite pulses were alternated with the standard cycle to suppress the second-order average Hamiltonian,[7] and to reduce the effects of pulse inhomogeneities and eddy currents in the metallic parts around the zero-field region. The experimental parameters were as follows: pulse lengths $\tau'=2$ μs, time intervals $\tau=3.6$ μs, cycle time 134.4 μs, acquisition dwell time 4×134.4 μs$=537.6$ μs. These values yield an ideal scaling factor of $23/70\approx0.33$ according to Eq. (36).

The distortions observed in the spectrum of Fig. 9(c) allow us to estimate the duration of the pulse transients and the amplitude of the eddy currents. We estimated the changes in k_1 and k_2 using a simplified model for the pulse transients (described by constant slopes, equal for the rising and falling edges) and for the eddy currents (described during each evolution period by a constant field along the orientation of the last applied pulse). Under these conditions, the 12 π paths defined by the sequence in SO(3) (see Fig. 6) are no longer explored at uniform speeds, and the scaling factors during the pulses are perturbed. The detailed calculations that will be given elsewhere[33] show that the first-rank scaling factor of the sequence (35) is not affected at all by the finite transient times or the eddy currents. The sequence is thus rather robust with respect to its decoupling capabilities. In contrast, for second-rank tensors the scaling factor is reduced both by the finite transient times and by the eddy currents. For instance, the effective scaling factor obtained in our experiment in Fig. 9(c) is about 0.28, i.e., 84% of the theoretical value of $23/70\approx0.33$. A numerical evaluation of the pulse-transient effects shows that, at the worst, the scaling factor would be $k_2=0.31$ for transient durations of 2 μs (which then means that, since the pulse length is also 2 μs, the pulse shape is triangular). On the other hand, the observed reduction of the scaling factor is obtained if the amplitude of the eddy currents is around 6.3% of the pulse amplitude. Actually, both pulse transients and eddy currents are present and they combine to yield the observed reduction of k_2. These estimates clearly show the importance of the experimental imperfections. It is not surprising then, that the fine structure of the original spectrum in Fig. 9(a) is distorted or lost under the decoupling sequence. Additional errors also arise from the third-order term in the average Hamiltonian[7] whose order of magnitude may be as high as 100 Hz, as evaluated from the cycle time and the highest frequency present in the system.

Despite the pulse-calibration difficulties and the pulse distortions, the ZFHF trajectory could be regarded a useful tool in designing icosahedral pulse-compensated schemes. However, the scaling factors averaged over the pulses in such sequences are positive and non-negligible, compared to the optimum time-reversal scalings: (1/3,1/5) vs $(-1/3,1/5)$ or $(1/6,-1/4)$ in the (k_1,k_2) plane (see Fig. 4). Since the total duration of the pulses must be much smaller than the cycle time, it becomes impractical to use this kind of compensation method for time-reversal sequences applied to strong local couplings, such as dipole–dipole interactions between protons in a solid sample. On our spectrometer, for example, the π pulses on protons were 2 μs long, giving a total of 24 μs for the six 2π-pulses needed in a ZFHF sequence. By combining these pulses with configurations on the $\cos\omega=-1/4$ sphere for optimum second-rank time reversal, we would get a modest scaling factor of $-1/20$ for a total cycle time of 48 μs. This is quite unacceptable for dipole–dipole interactions between protons that usually fall in the 50 kHz range. We have therefore explored other possibilities to avoid the difficulties associated with sequences of icosahedral type. An important class is provided by the cubic sequences,[18] where the set of configurations is restricted to those generated by combinations of $\pi/2$ pulses along the three axes. A companion article is devoted to this topic.[34]

VIII. CONCLUSIONS

We have shown theoretically that isotropic coherent manipulations (decoupling, time reversal) are possible in zero-field NMR on powder samples, and we have discussed the limits and the main features for optimum δ-pulse sequences in homonuclear spin systems. Both the first-rank interactions (such as residual fields) and the second-rank interactions (dipolar or quadrupolar couplings) can be isotropically scaled. The scaling factors of a given isotropic scheme can be different for the two types of interactions, although they are not completely independent. In any case, the first-rank scaling factors are between $-1/3$ and 1, whereas those for the second-rank fall between $-1/4$ and 1. Due to experimental limitations the application of those techniques was shown for one simple case only, and more practical schemes based on $\pi/2$ pulses are developed in the second paper.[34]

The potential applications of this work will be primarily in further expansion of ZF-NMR methods.[18,19] Two cases of isotropic scaling can be considered particularly useful: decoupling and time reversal. In the homonuclear case, the decoupling according to the rank of the interactions allows us to eliminate the usually disturbing effects of nonzero residual fields. The decoupling is also useful in the heteronuclear case, because various local interactions can be made to behave as tensors of different ranks due to different values of the magnetogyric ratios.[18] Time reversal is probably the most interesting of the new possibilities, because it allows us to design a zero-field analogue of the HF-NMR technique called multiple-quantum NMR.[10] This technique that we shall call ''multipolar zero-field NMR,'' should yield simpler

spectra for many-spin systems by reducing the number of transitions (like in multiple-quantum NMR), while still preserving the isotropy of spectra.

Another closely related spectroscopy that may profit from the isotropic techniques is nuclear quadrupolar resonance (NQR). Apart from the problem of isotropic manipulation, which is identical to the ZF-NMR case, NQR creates yet another difficulty: The local interactions are usually too strong to allow the excitation of the whole spectrum by currently available magnetic-field pulses. Radiofrequency pulses are thus applied to excite and observe the vicinity of some transitions only. The effect of such pulses can be considered similar to that of dc pulses but truncated so as to retain the matrix elements corresponding to the transition under study. This truncation effect of the excitation field by the local interaction is orientation dependent. In contrast to the zero-field situation where a dc pulse generates a rotation independent of the crystallite orientation, the allowed manipulations in NQR are not rotations and are not isotropic. The configuration space and the trajectories are so complex, that generating coherent averaging schemes with such tools seems hopeless. However, in the case of a spin 1 or 3/2, for instance, it is possible to ''untruncate'' an rf pulse by simultaneously applying a matched dc pulse in the same direction. Thus reducing the effect of the global pulse to a simple, isotropic rotation of the spins is possible, and any isotropic technique based on rotations can be used. Though such methods would be rather demanding experimentally, potential applications of decoupling, multipolar analysis, or even imaging, would be important.

An interesting theoretical question is that of the class of systems that can be time reversed.[9] Intuitively, it could be argued that this is possible on two-dimensional systems only, as in the previously known examples from HF-NMR where the truncation formally restricts the coherences to the transverse plane. The problem was raised twenty years ago[9] and is still unsolved, but we have now, with the negative isotropic scalings, added a new broad class of systems which are basically three dimensional. Thus it seems that the dimensionality is certainly not a limiting factor and that probably few, if any, restrictions exist for time reversal of spin couplings, provided one has some appropriate experimental means of manipulating the coherences.

APPENDIX: CALCULATION OF THE MAGNETIC-FIELD PULSES IN ICOSAHEDRAL SEQUENCES

We assume that the configurations represent *active* rotations of the Hamiltonians, in a *right-handed* reference frame.[25] This assumption is not important for the general theory of icosahedral sequences as given in Secs. III and IV (passive rotations are just opposite to active rotations, and the icosahedral sequences always contain opposite configurations). However, it is an important point to explicitly compute the pulse characteristics, because the trajectory obtained by reverting the pulses of an icosahedral sequence is not necessarily icosahedral.

The question whether rotations are active or passive is seldom important in HF-NMR,[1,7] because the Hamiltonian is truncated and the pulses are confined to the transverse plane. Then, the transformation from active to passive pulses can be accounted for by a simple π phase shift of the transmitter. This is not the case in ZF-NMR, and to avoid any confusion, the *pulses will be given as the active rotations* that are deduced from the configurations using Eq. (2). To translate the spin rotations into magnetic field pulses in the spectrometer, all the possible inversion sources must also be taken into account: signs in the Shrödinger equation, the Hamiltonians, and the magnetogyric ratio, and polarities of the pulsed coils around the sample. Assuming a *positive magnetogyric ratio* and a *right-handed positive system of pulsed coils*, the Hamiltonian and the propagator in the spin space for a dc pulse are[1,7]

$$H=-\gamma\mathbf{I}\cdot\mathbf{B}, \tag{A1a}$$

$$P=\exp[-iHt]=\exp[i\gamma\mathbf{I}\cdot\mathbf{B}t]=\exp[i\alpha\mathbf{I}\cdot\mathbf{n}], \tag{A1b}$$

where $\mathbf{B}$ is the magnetic field vector along direction $\mathbf{n}$, and α is the pulse angle. The operator P is an active rotation by angle α along direction $-\mathbf{n}$ [or a passive rotation $(\alpha,\mathbf{n})$]. This just means that spins of positive magnetogyric ratio precess *counterclockwise* in a magnetic field.

The icosahedral pulse sequences (18) and (19) are defined by 12 vertices of an icosahedron drawn on a sphere at constant ω inside the configuration space SO(3). This is shown in Fig. 3, where we chose the icosahedron to be embedded in the reference frame with C_2 symmetry axes along X, Y, and Z. The rotation axes of the configurations are then given by the normalized vectors

$$\mathbf{n}_i=\pm\left(\pm\sqrt{\frac{5-\sqrt{5}}{10}},0,\sqrt{\frac{5+\sqrt{5}}{10}}\right)\ \&\text{c.c.}, \tag{A2}$$

where c.c. stands for the cyclic permutations (Z,X,Y) and (Y,Z,X). This choice of the reference frame will simplify the calculation of the pulses, provided that we choose, as in Fig. 3, a C_3-symmetric trajectory along the $\langle 111\rangle$ magic direction (it can be seen that this is the highest possible symmetry available for a 12-pulse path). The path shown in Fig. 3 is the only one that displays such a symmetry and joins the neighboring vertices of the icosahedron.

The pulse lengths and directions are deduced from Eq. (2) according to the formulas giving the angle and axis for the combination of two (active) rotations[25]

$$R(\alpha,\mathbf{n})=R(\alpha_2,\mathbf{n}_2)\cdot R(\alpha_1,\mathbf{n}_1), \tag{A3a}$$

$$\cos(\alpha/2)=\cos(\alpha_1/2)\cos(\alpha_2/2)-(\mathbf{n}_1\cdot\mathbf{n}_2)\sin(\alpha_1/2)\sin(\alpha_2/2), \tag{A3b}$$

$$\mathbf{n}\sin(\alpha/2)=\mathbf{n}_1\sin(\alpha_1/2)\cos(\alpha_2/2)+\mathbf{n}_2\sin(\alpha_2/2)\cos(\alpha_1/2)-(\mathbf{n}_1\times\mathbf{n}_2)\sin(\alpha_1/2)\sin(\alpha_2/2). \tag{A3c}$$

If we select for $\mathbf{n}_1$ and $\mathbf{n}_2$ the vertices labeled 1 and 2 in Fig. 3, as given by Eq. (A2), we find the pulse

$$P_{1\to 2}=R(\alpha,\mathbf{n})=R(\omega,-\mathbf{n}_2)\cdot R(\omega,\mathbf{n}_1), \tag{A4}$$

according to Eq. (2). From Eq. (A3) and after some elementary transformations we find the pulse angle and direction

$$\cos\,\alpha=\frac{(3-\sqrt{5})\cos^2\,\omega+4\,\cos\,\omega+(\sqrt{5}-2)}{5}, \tag{A5a}$$

$$\mathbf{n}_{1\to 2}\,\sin(\alpha/2)=\left(-\sqrt{\frac{5-\sqrt{5}}{10}}\,\sin\,\omega,\ \frac{1}{\sqrt{5}}\,(1-\cos\,\omega),0\right). \tag{A5b}$$

$\mathbf{n}_{1\to 2}$ is thus confined to the XY plane, and its orientation can be described by an angle θ, according to

$$\mathbf{n}_{1\to 2}=(u_1,v_1,w_1)=(-\cos\,\theta,\sin\,\theta,0)=\left(-\sqrt{\frac{5+\sqrt{5}}{2}}\,\sqrt{\frac{1+\cos\,\omega}{4+\sqrt{5}+\cos\,\omega}},\ \sqrt{\frac{3+\sqrt{5}}{2}}\,\sqrt{\frac{1-\cos\,\omega}{4+\sqrt{5}+\cos\,\omega}},0\right). \tag{A6}$$

All the pulses between the vertices in Fig. 3 can be deduced from that between 1 and 2 using the appropriate rotation that brings the (1,2) edge to the (i,j) edge. For (2,3), (3,4), and (4,5) we use rotations by $-2\pi/3$ around face (1,2,3), $2\pi/3$ around (1,1,−1), and $2\pi/3$ around face (1,4,5), respectively. Owing to the C_3 symmetry of the trajectory, the remaining eight pulses are found by applying cyclic permutations of the coordinates. Using explicit expressions for the rotations, and after some elementary, though lengthy, algebraic manipulations, we found that

$$\mathbf{n}_{2\to 3}=(u_2,v_2,w_2)=\begin{pmatrix} -\frac{1}{2} & \frac{\sqrt{5}+1}{4} \\ -\frac{\sqrt{5}+1}{4} & -\frac{\sqrt{5}-1}{4} \\ -\frac{\sqrt{5}+1}{4} & -\frac{1}{2} \end{pmatrix}\begin{pmatrix} -\cos\,\theta \\ \sin\,\theta \end{pmatrix}, \tag{A7a}$$

$$\mathbf{n}_{3\to 4}=(u_3,v_3,w_3)=(\sin\,\theta,0,\cos\,\theta), \tag{A7b}$$

$$\mathbf{n}_{4\to 5}=(u_4,v_4,w_4)=\begin{pmatrix} \frac{\sqrt{5}+1}{4} & -\frac{\sqrt{5}-1}{4} \\ \frac{\sqrt{5}-1}{4} & -\frac{1}{2} \\ \frac{1}{2} & \frac{\sqrt{5}+1}{4} \end{pmatrix}\begin{pmatrix} -\cos\,\theta \\ \sin\,\theta \end{pmatrix}. \tag{A7c}$$

Above certain value of ω, the distances between the neighboring vertices on the trajectory of Fig. 3 (measured as the pulse length) may become larger than those between the opposite vertices. This happens when $\alpha>2(\pi-\omega)$, and using Eq. (A5a) this is equivalent to

$$\cos\,\omega<-\frac{4+\sqrt{5}}{11}, \tag{A8}$$

or $\omega\approx 124.54°$. Above this value, a more efficient trajectory (preserving the C_3 symmetry) is 1,2,8,11,5,6,12,3,9,10,4,3. The (2,8) and (11,5) pulses are both of angle $2(\pi-\omega)$ and along the $-\mathbf{n}_2$ and $-\mathbf{n}_{11}$ directions respectively, while the (8,11) pulse again is deduced from the (1,2) pulse by a rotation of $-2\pi/3$ around face (6,9,10)

$$\mathbf{n}_{8\to 11}=(u_3',v_3',w_3')=\begin{pmatrix} -\frac{\sqrt{5}-1}{4} & \frac{1}{2} \\ \frac{1}{2} & \frac{\sqrt{5}+1}{4} \\ \frac{\sqrt{5}+1}{4} & -\frac{\sqrt{5}-1}{4} \end{pmatrix}\begin{pmatrix} -\cos\,\theta \\ \sin\,\theta \end{pmatrix}. \tag{A9}$$

Specific pulse values for some useful scaling factors have been explicitly computed using Eqs. (A5a), (A6), (A7), and (A9). The results are summarized in Table I.

ACKNOWLEDGMENTS

We are grateful to J. Sachleben for his help with the experiments. This work was supported by the Director, Office of Energy Research, Office of Basic Energy Sciences, Materials Sciences Division of the U.S. Department of Energy under Contract No. DE-AC03-76SF00098. A.L. also acknowledges financial support from the Commissariat á l'Energie Atomique, France, and from the North-Atlantic Treaty Organization (Grant No. 68C89FR).

[1] A. Abragam, *Principles of Nuclear Magnetism* (Clarendon, Oxford, 1961); C. P. Slichter, *Principles of Magnetic Resonance* (Springer-Verlag, Berlin, 1990), 3rd ed.
[2] R. R. Ernst, G. Bodenhausen, and A. Wokaun, *Principles of NMR in One and Two Dimensions* (Oxford Scientific, Oxford, 1987); C. A. Fyfe, *Solid State NMR for Chemists* (C.F.C., Guelph, 1983).
[3] E. R. Andrew, A. Bradbury, and R. G. Eades, Nature (London) **182**, 1659 (1958); I. J. Lowe, Phys. Rev. Lett. **2**, 285 (1959).
[4] J. S. Waugh, L. M. Huber, and V. Haeberlen, Phys. Rev. Lett. **20**, 180 (1968); U. Haeberlen and J. S. Waugh, Phys. Rev. **175**, 453 (1968).
[5] A. Llor and J. Virlet, Chem. Phys. Lett. **152**, 248 (1988); B. F. Chmelka, K. T. Mueller, A. Pines, J. Stebbins, Y. Wu, and J. W. Zwanziger, Nature (London) **339**, 42 (1989).
[6] A. Samoson, E. Lippmaa, and A. Pines, Mol. Phys. **65**, 1013 (1988).
[7] M. Mehring, *Principles of High Resolution NMR in Solids*, 2nd ed. (Springer, Berlin, 1983); U. Haeberlen, *Advances in Magnetic Resonance, Suppl. 1* (Academic, New York, 1976).
[8] E. L. Hahn, Phys. Rev. **80**, 580 (1950).
[9] W.-K. Rhim, A. Pines, and J. S. Waugh, Phys. Rev. Lett. **25**, 218 (1970); Phys. Rev. B **3**, 684 (1971); K. Takegoshi and C. A. McDowell, Chem. Phys. Lett. **116**, 100 (1985).
[10] D. P. Weitekamp, Adv. Magn. Reson. **11**, 111 (1983); M. Munowitz and A. Pines, Adv. Chem. Phys. **LXVI**, 1 (1987).
[11] D. P. Weitekamp, A. Bielecki, D. Zax, K. Zilm, and A. Pines, Phys. Rev.

Lett. **50**, 1807 (1983); D. Zax, A. Bielecki, K. Zilm, A. Pines, and D. P. Weitekamp, J. Chem. Phys. **83**, 4877 (1985).
[12] T. P. Das and E. L. Hahn, *Solid State Physics, Supplement No. 1* (Academic, New York, 1958).
[13] R. Tycko, J. Magn. Reson. **75**, 193 (1987); R. Tycko, Phys. Rev. Lett. **60**, 2734 (1988); B. Q. Sun and A. Pines, J. Magn. Reson. A **109**, 157 (1994).
[14] R. Tycko, J. Chem. Phys. **192**, 5776 (1990).
[15] M. Bloom and N. E. Norberg, Phys. Rev. **93**, 638 (1954); E. L. Hahn and B. Herzog, *ibid.* **93**, 639 (1954); W. G. Proctor and W. H. Tantilla, *ibid.* **98**, 1854 (1955); W. G. Proctor and W. A. Robinson, *ibid.* **102**, 1183 (1956).
[16] R. A. Marino and S. M. Klainer, J. Chem. Phys. **67**, 3388 (1977); R. S. Cantor and J. S. Waugh, *ibid.* **73**, 1054 (1980); D. Ya. Osokin, Phys. Status Solidi B **102**, 681 (1981); V. L. Ermakov and D. Ya. Osokin, Mol. Phys. **53**, 1335 (1984).
[17] R. Kreis, D. Suter, and R. R. Ernst, Chem. Phys. Lett. **118**, 120 (1985); *ibid.* **123**, 154 (1986).
[18] C. J. Lee, D. Suter, and A. Pines, J. Magn. Reson. **75**, 110 (1987).
[19] A. Llor, D. Sc. thesis (in French), Université Paris XI, Orsay, 1987.
[20] A. Llor, Z. Olejniczak, J. Sachleben, and A. Pines, Phys. Rev. Lett. **67**, 1989 (1991).
[21] Throughout the following, we shall deal only with zeroth-order average Hamiltonians (Ref. 7), but, according to a more consistent terminology, we shall refer to them as first-order average Hamiltonians, all the next terms also being shifted by one unit [see W. R. Salzman, J. Chem. Phys. **85**, 4605 (1986); M. M. Maricq, *ibid.* **86**, 5647 (1987)].
[22] E. P. Wigner, *Group Theory and its Applications to the Quantum Mechanics of Atomic Spectra* (Academic, New York, 1959); M. Hamermesh, *Group Theory and its Applications to Physical Problems* (Dover, New York, 1989).
[23] J.-Q. Chen, *Group Representation Theory for Physicists* (World Scientific, Singapore, 1989).
[24] G. J. Bowden, J. P. D. Martin, and F. Separovic, Mol. Phys. **70**, 581 (1990).
[25] D. A. Varshalovich, A. N. Moskalev, and V. K. Khersonskii, *Quantum Theory of Angular Momentum* (World Scientific, Singapore, 1988).
[26] S. L. Sobolev, Dokl. Akad. Nauk SSSR **146**, 310 (1962); S. L. Sobolev, Dokl. Akad. Nauk SSSR **146**, 770 (1962).
[27] A. H. Stroud, *Approximate Calculation of Multiple Integrals* (Prentice-Hall, Englewood Cliffs, 1971); A. M. Tam, Ph.D. dissertation, University of California, Berkeley, 1982.
[28] A. Pines, *NMR in Physics, Chemistry and Biology: Illustrations of Bloch Legacy*, Bloch Symposium, Stanford, 1989; transcripted in *Conductivity and Magnetism. The Legacy of Felix Bloch*, edited by W. A. Little (World Scientific, Singapore, 1990).
[29] A. Bax, N. M. Szeverenyi, and G. E. Maciel, J. Magn. Reson. **52**, 147 (1983).
[30] M. Lee and W. I. Goldburg, Phys. Rev. A **140**, 1261 (1965).
[31] M. Luzar, A. M. Thayer, and A. Pines, J. Magn. Reson. **73**, 459 (1987); A. M. Thayer, M. Luzar, and A. Pines, Liq. Cryst. **2**, 241 (1987).
[32] A. Bielecki, D. Zax, K. Zilm, and A. Pines, Rev. Sci. Instrum. **57**, 393 (1986).
[33] A. Llor, Z. Olejniczak, and A. Pines (unpublished).
[34] A. Llor, Z. Olejniczak, and A. Pines, J. Chem. Phys. **103**, 3982 (1995).